



## Full Text View

[Volume 29, Issue 7 \(July 1999\)](#)

### Journal of Physical Oceanography

Article: pp. 1425–1441 | [Abstract](#) | [PDF \(1.07M\)](#)

## Dynamics of the Mediterranean Salinity Tongue

**James C. Stephens and David P. Marshall**

*Department of Meteorology, University of Reading, Reading, United Kingdom*

(Manuscript received March 25, 1998, in final form July 16, 1998)

DOI: 10.1175/1520-0485(1999)029<1425:DOTMST>2.0.CO;2

### ABSTRACT

A reduced-gravity planetary-geostrophic model of the North Atlantic consisting of two active layers overlying a motionless abyss is developed to investigate the effect of the wind field in shaping the dynamics of the Mediterranean salinity tongue. The model is driven by climatological winds and eastern boundary ventilation in a basin of realistic geometry and includes a parameterization of meddies.

The upper-layer depth from the model shows a clear similarity to observations, both in terms of the location and intensity of the subtropical gyre and also the position of the outcropping line in the northern basin. Potential vorticity in layer two reproduces the sweep of potential-vorticity contours southwestward from the eastern boundary and extending westward into the interior, and provides the pathways along which Mediterranean Water spreads into the model interior.

The authors solve for the steady salinity field in the second layer, including sources of Upper Labrador Sea Water and Antarctic Intermediate Water on the isopycnal surface. The shape and spreading latitude of the model salinity tongues bear a striking resemblance to observations. Both the wind forcing and the occurrence of a mean transport of Mediterranean Water away from the eastern boundary are crucial in obtaining a realistic salinity tongue. The salinity tongues are remarkably stable to variations in the Peclet number.

A simple parameterization of meddies in the model is also included. Where meddies are dissipated locally by collisions with topographic seamounts, for example, they may generate large recirculations extending across to the western boundary. The net effect of these recirculations is to shift the salinity tongue equatorward.

#### Table of Contents:

- [Introduction](#)
- [Dynamical model](#)
- [Salinity tongues](#)
- [Meddies](#)
- [Discussion](#)
- [REFERENCES](#)
- [APPENDIX](#)
- [FIGURES](#)

#### Options:

- [Create Reference](#)
- [Email this Article](#)
- [Add to MyArchive](#)
- [Search AMS Glossary](#)

#### Search CrossRef for:

- [Articles Citing This Article](#)

#### Search Google Scholar for:

- [James C. Stephens](#)
- [David P. Marshall](#)

A tongue of warm and salty water known as the Mediterranean salinity tongue (MST) is the most prominent feature of the North Atlantic at middepths. It sets the temperature–salinity structure of a large part of the interior ocean in this region. [Figure 1](#) shows salinity on potential density surfaces  $\sigma_1 = 31.85$  (depth  $\sim 600$  m at the eastern boundary, the upper limit of the MST) and  $\sigma_1 = 32.35$  (depth  $\sim 1500$  m). On  $\sigma_1 = 31.85$  there is a pronounced northward as well as a westward extension of the MST. Upper Labrador Sea Water (ULSW,  $S \approx 34.88$  psu) can be seen in the northwest of the basin comprising part of the deep western boundary current, and also Antarctic Intermediate Water (AAIW,  $S \approx 34.98$  psu) spreading northward from the southern boundary. On  $\sigma_1 = 32.35$  the spreading of the MST is less extensive and there is less northward spreading.

The Mediterranean Water (MW) signal is actually extended to depths of 3000 m by vertical mixing processes such as salt fingering, but we will hereafter concern ourselves mainly with the upper MST between  $\sim 600$  m and 1500 m; that which lies below 1500 m we will refer to as the lower MST.

### *a. Undercurrent*

The MST has its origin in the Strait of Gibraltar, where there is an exchange flow between the Mediterranean Sea and the Atlantic Ocean. The Mediterranean outflow mixes strongly with the overlying North Atlantic Central Water (NACW) and descends the continental slope to form an adjusted gravity current known as the Mediterranean Undercurrent (MU). The transport of the outflow has been estimated by [Baringer and Price \(1997a\)](#) to increase from 0.7 Sv ( $\text{Sv} \equiv 10^6 \text{ m}^3 \text{ s}^{-1}$ ) at the western end of the Strait of Gibraltar to 1.9 Sv within the western Gulf of Cadiz (GOC) by entrainment of NACW. Many estimates of the transport after mixing have been made, varying from 1.2 Sv by [Lacombe \(1971\)](#) to 6.5 Sv by [Howe \(1984\)](#), although 2–3 Sv is typical. The MU separates into two distinct cores during its descent and reaches neutral buoyancy near Cape St. Vincent ( $37^\circ\text{N}$ ,  $9^\circ\text{W}$ ) at depth around 1000 m ([Baringer and Price 1997b](#)). Beyond Cape St. Vincent the two cores of the MU behave differently. The upper core ( $\sigma_1 = 31.85$ ) follows the topography northward along the Portuguese coast as a slope current ([Kase and Zenk 1996](#)), whereas the lower core ( $\sigma_1 = 32.25$ ) rises above the topography and meanders west and northwestward forming large boluses of Mediterranean Water ([Zenk and Armi 1990](#)).

[Reid \(1979\)](#) concluded from silica data that the MU flows directly into the Nordic seas, helping to maintain their high salinity. This picture however is at odds with [McCartney and Mauritzen \(1999, manuscript submitted to \*Deep-Sea Res.\*, hereafter MM99\)](#), who propose that the last remnants of the MU, whose volume transport decreases northward, are “pinched off” at Porcupine Bank ( $\sim 50^\circ\text{N}$ ) by the North Atlantic Current, which then branches northward and is modified by winter convection before flowing directly into the Nordic seas.

### *b. Meddies*

The discovery of an intense eddy containing water of Mediterranean origin in the Bahamas by [McDowell and Rossby \(1978\)](#) led to the investigation and discovery of many more such lenses, termed “meddies.” These are anticyclonic eddies, typically 20–100 km across ([Bower et al. 1995](#)), which may extend over the entire depth of the MST. They are very coherent, characterized by positive salinity anomalies of at least 0.4 psu ([Richardson et al. 1991](#)) and rapid core rotations ( $\sim 0.3 \text{ m s}^{-1}$ ; [Bower et al. 1997](#)). [Bower et al. \(1997\)](#) identified Cape St. Vincent and the Estremadura Promontory ( $39^\circ\text{N}$ , also known as the Tagus Plateau) as important meddy formation sites and estimated a formation rate of 15–20 meddies per year from float data. The presence of preferred sites indicates that meddies are likely formed by some combination of disturbances due to canyons and/or sharp corners in the continental slope ([D’Asaro 1988](#)) upon which the MU flows. Support for this is found by [Bower et al. \(1995\)](#).

Meddies may be long-lived, decaying only slowly due to double-diffusive and turbulent processes ([Armi et al. 1989](#)), or they may collide with topographic seamounts, possibly catastrophically [[Richardson et al. \(1989\)](#), [Richardson and Tychensky \(1998, hereafter, RT98\)](#), [Shapiro et al. \(1995\)](#)]. The Great Meteor Seamount (GMS) chain ( $29^\circ$ – $35^\circ\text{N}$ ,  $28^\circ\text{W}$ ) was identified as a possible important site for this by [Richardson et al. \(1989\)](#). Meddies may also interact with the Azores Current (RT98) or other (m)eddies. [Richardson et al. \(1989\)](#) estimated, based on a notional meddy formation rate and lifetime, that meddies contribute about 25% of the salt anomaly flux into the North Atlantic; [Arhan et al. \(1994\)](#) produced an estimate of 55%, based on a rough calculation from a single hydrographic section. It seems likely therefore that the dissipation of meddies is important in determining the location and shape of the salinity tongue, particularly where this dissipation is local and enhanced by collisions with seamounts for example.

### *c. Previous theories of the salinity tongue*

[Richardson and Mooney \(1975\)](#) examined the effect of different advective–diffusive balances in a numerical tracer model,

combining the velocity field from a barotropic wind-driven gyre with an eastern-boundary salinity source. They were able to generate a realistically shaped salinity tongue in the model for certain diffusivities of salt, but their mean velocities were too large. [Armi and Haidvogel \(1982\)](#) demonstrated tonguelike features through the use of zonally enhanced mixing coefficients in the absence of a mean flow. [Spall et al. \(1993\)](#) supports the presence of zonally enhanced mixing and demonstrates that eddy mixing may play a crucial role in the dynamical balance. This hinges on the weak role of a mean flow at the depths of the MST. The mean flow is certainly small; [Zenk and Müller \(1988\)](#) find no significant mean current in seven years of data from 1000-m depth at 32°N, 22°W in the Canary Basin [see [Müller and Siedler \(1992\)](#) for a more recent nine year analysis of the same mooring]. The magnitude of the mean flow, if there is one at all, clearly needs to be determined.

There has been much work attempting to explain the northward spreading of the MST. Proposed mechanisms have included Ekman suction in the subpolar gyre ([Schopp and Arhan 1986](#)), double-diffusive salt fingering from the base of the upper MST ([Arhan 1987](#); [Spall 1999](#)) and damped Rossby waves emanating from the eastern boundary ([Tziperman 1987](#)). These studies were motivated by [Saunders \(1982\)](#), who used hydrographic data to infer northward absolute velocities from the eastern boundary to 30°W, between 36°N and 50°N and depth 500 and 1000 m. However, this result relies on a level of no motion chosen to satisfy Sverdrup balance. A more recent inverse calculation ([Paillet and Mercier 1997](#)) shows no interior northward velocities at 1000-m depth, apart from near the surface at 48°N. In [Fig. 2](#) we reproduce section-averaged current profiles (as per [Saunders 1982](#)) computed from the data of [Paillet and Mercier \(1997\)](#) for latitudes 32°–48° N. In contrast to [Saunders \(1982\)](#), the only northward velocities are north of ~48°N in the surface layers, where the North Atlantic Current impinges upon the eastern boundary and branches northward as part the subpolar gyre.

Comparing the results of [Saunders \(1982\)](#) and [Paillet and Mercier \(1997\)](#), it seems that although there is a consensus on the existence of southward flow at the depths of the lower MST, there is a lack of consensus on the velocity field at the depths of the upper MST. It does seem somewhat surprising that there has been so much emphasis on explaining the northward spreading of the MST in terms of northward interior velocities, when this can so readily be achieved via the Mediterranean Undercurrent, which flows northward along the continental shelf and could ventilate the interior through instability processes.

#### *d. Motivation for the present study*

While diabatic processes may be important in describing the detailed structure of the MST, at leading order one might expect the circulation to be well described by adiabatic flow along potential vorticity contours. [Figure 3](#) shows the depths of the  $\sigma_1 = 31.85$  and  $\sigma_1 = 32.35$  potential density surfaces (corresponding to the salinity tongues shown in [Fig. 1](#)). There is a bowl-shaped depression of the  $\sigma_1 = 31.85$  surface toward the west of the subtropical gyre, and the isopycnal surface outcrops in the subpolar gyre to the north. This behavior is in accordance with the wind-driven theories of [Rhines and Young \(1982a\)](#) and [Luyten et al. \(1983\)](#) and leads to a northeast–southwest orientation in the potential vorticity contours in the depth range of the upper MST (as shown in [Fig. 4](#)). This suggests that the wind field plays a direct role in shaping the potential vorticity field at the depths of the upper MST. We imagine that these potential vorticity contours can be ventilated by the Mediterranean Undercurrent and by meddies. The MW will interact with ULSW entering from the western boundary and AAIW entering from the south. We do not consider the lower MST (below 1500 m), at the depths of which vertical mixing by double diffusion ([Spall 1999](#)) and topographic influences appear to be important—the dynamics of the lower MST has recently been considered in some detail by [Spall \(1999\)](#).

In this paper we develop a simple dynamical model with the specific aims of understanding:

- The role of the wind field and eastern-boundary ventilation in shaping the upper MST.
- The sensitivity of the MST to uncertain isopycnal mixing coefficients, and to the extent of potential vorticity homogenization within deep recirculation gyres.
- The impact of meddies and other water masses (ULSW, AAIW) on the structure of the MST.

In [section 2](#) we develop an inviscid, adiabatic model driven by climatological-mean winds and eastern boundary ventilation in a North Atlantic basin of realistic geometry. In [section 3](#) we develop a tracer model, in which we solve for the steady salinity field in the presence of MW, ULSW, and AAIW, and a parameterization of eastern and western boundary currents. In [section 4](#) we consider the role of meddies in driving a modification to the mean flow. A discussion and summary of the results is given in [section 5](#).

## **2. Dynamical model**

### *a. Dynamical balances*

A 2.5-layer model of the North Atlantic is constructed in a domain extending from 10°N to 60°N, 0° to 80°W. The model has a realistic coastal configuration corresponding to 1000-m bathymetry. The configuration of the model layers is shown in [Fig. 5](#). The model dynamics are steady, geostrophic, hydrostatic, and in Sverdrup balance and closely follow the formulations of [Rhines and Young \(1982b\)](#) and [Luyten et al. \(1983\)](#). The solutions we compute represent only the interior ocean and not the eastern and western boundary currents, which exist outside the model domain.

For our system, in which layer 3 is taken to be infinitely deep and motionless, hydrostatic balance gives the dynamic pressures as

$$\frac{p_1}{\rho_0} = -\gamma_1 z_2 - \gamma_2 z_3, \quad (1)$$

$$\frac{p_2}{\rho_0} = -\gamma_2 z_3,$$

where

$$\gamma_n = \frac{(\rho_{n+1} - \rho_n)g}{\rho_0} \quad (2)$$

are the reduced gravities,  $p_n$  is pressure,  $\rho_n$  is density,  $z_n$  is the height of the interface separating layers  $n$  and  $n + 1$ ,  $g$  is the gravitational acceleration,  $\rho_0$  is a constant reference density, and  $n$  is a layer index.

Geostrophic balance is expressed in spherical coordinates as

$$\begin{aligned} f u_n &= -\frac{1}{\rho_0 R} \frac{\partial p_n}{\partial \theta}, \\ f v_n &= \frac{1}{\rho_0 R \cos \theta} \frac{\partial p_n}{\partial \phi}, \end{aligned} \quad (3)$$

where  $u_n$  and  $v_n$  are velocities,  $R$  is the earth's radius, and  $\theta$  and  $\phi$  are latitude and longitude respectively. The Coriolis parameter is given by  $f = 2\Omega \sin \theta$ .

The model is driven by an Ekman pumping field,  $w_{\text{Ek}}$  (shown in [Fig. 6](#)) computed from the seasonally averaged [DaSilva et al. \(1994\)](#) climatology as

$$w_{\text{Ek}} = -\frac{1}{\rho_0} \mathbf{k} \cdot \nabla \times \left( \frac{\boldsymbol{\tau}}{f} \right), \quad (4)$$

where  $\boldsymbol{\tau}$  is a surface wind stress.

### b. Sverdrup balance

Sverdrup balance is expressed

$$\beta[\mathbf{v}_1 h_1 + \mathbf{v}_2 h_2] = f w_{\text{Ek}}, \quad (5)$$

where

$$\beta = \frac{1}{R} \frac{\partial f}{\partial \theta} \quad (6)$$

is the meridional gradient of the Coriolis parameter. Substituting (3) into (5), and integrating with respect to  $\Phi$ , we obtain

$$\gamma_1 z_2^2 + \gamma_2 z_3^2 = -2 \frac{f^2}{\beta} \int_{\phi_W}^{\phi_E} w_{EK} R \cos\theta \partial\phi + \gamma_1 \hat{Z}_2^2 + \gamma_2 \hat{Z}_3^2, \quad (7)$$

where  $\phi_W$  and  $\phi_E$  are the western and eastern limits of the integration, and  $\hat{Z}_2$  and  $\hat{Z}_3$  are the values of  $z_2$  and  $z_3$  at  $\Phi = \phi_E$ . We obtain a steady solution by integrating (7) across the basin from the eastern boundary, assuming no motion in layer two in the first instance since the eastern boundary condition prevents flow along potential vorticity contours that intersect it. The region for which this occurs is known as the shadow zone (Luyten et al. 1983). We then examine the potential vorticity contours a posteriori to determine those contours for which our initial assumption was invalid; in this region we require a different approach.

### c. Flow in layer two

Potential vorticity in layer two is defined

$$q_2 = \frac{f}{z_2 - z_3}. \quad (8)$$

Potential vorticity contours, which, sufficiently distorted by the wind field, are able to close in on themselves against the western boundary, are not subject to the eastern boundary condition. Rhines and Young (1982a) argued that motion is able to occur in this region, known as the closed pool; they hypothesized that the action of turbulent processes serves to homogenize  $q_2$  in the closed pool to its value on the outer perimeter. These turbulent processes are negligible in the zero-order dynamical balance and it is only their action over a long timescale that allows them to homogenize the potential vorticity.

The occurrence, or otherwise, of a homogenized region (HR) has been a matter of great controversy in recent years. Figure 4 shows some evidence for an HR, and in the case of our model there is an extensive region of closed contours against the western boundary in layer two. If we homogenize  $q_2$  within these closed contours, then we will obtain a flow in the western basin in layer two; without homogenization of  $q_2$  there will be no flow in this region. We choose out of interest to explore both of these extremes and note their effects on the model fields.

If we choose to homogenize, we can solve for the flow inside the closed pool in which the Sverdrup transport is carried over both layers one and two as follows. In the pool region we require [from (8)]

$$z_3 = z_2 - \frac{f}{q_h}, \quad (9)$$

where  $q_h$  is the value of  $q$  at the boundary of the HR. Substituting (9) into (7) we obtain a quadratic for  $z_2$  as follows:

$$\begin{aligned} & [\gamma_1 + \gamma_2] z_2^2 - \left[ \frac{2f\gamma_2}{q_f} \right] z_2 + 2 \frac{f^2}{\beta} \int_{\phi}^{\phi_B} w_E R \cos\theta \partial\phi \\ & + \gamma_2 \left[ \frac{f^2}{q_h^2} - \hat{Z}_3^2 \right] - \gamma_1 \hat{Z}_2^2 = 0. \end{aligned} \quad (10)$$

The physical root of (10) yields  $z_2$  and resubstitution into (9) and (8) yields  $z_3$ ,  $q_1$ , and  $q_2$  in the pool.

### d. Typical solution



Fields from a typical solution are shown in [Fig. 7](#) for the homogenized case. Here  $\hat{Z}_2 = -600$  m is chosen to represent the upper limit of the MST shown on the  $\sigma_1 = 31.85$  surface of [Lozier et al. \(1995\)](#), as can be seen from the pressure field on that surface ([Fig. 3](#)). Here  $\hat{Z}_3 = -1300$  m is chosen as the lower limit of the MST in the model since it is our intention in this 2.5-layer model to focus our attention on the upper MST. The reduced gravities,  $\gamma_1 = 0.005$  m s<sup>-2</sup> and  $\gamma_2 = 0.0025$  m s<sup>-2</sup> are diagnosed from hydrographic data presented in [Chérubin et al. \(1997\)](#).

The depth of the  $z_2$  surface (the base of the upper layer) exhibits a clear similarity to the depth of the  $\sigma_1 = 31.85$  surface in [Fig. 3](#), both in terms of the location and intensity of the subtropical gyre and also the position of the outcrop line in the subpolar gyre. The  $z_2$  surface outcrops in the subpolar gyre in the manner of [Luyten et al. \(1983\)](#); beyond this line the Sverdrup transport is carried entirely in layer two, although in contrast to the study of [Schopp and Arhan \(1986\)](#), there is no ventilation of layer two since the outcrop line is a streamline.

The layer two velocities in the outcropped region are too strong and can cause the  $z_3$  surface (not shown) to outcrop too; the outcropping of the  $z_3$  surface (the base of layer two) is unrealistic and a consequence of the limited vertical structure of our model. North of this outcrop the Sverdrup transport is carried by the lowest layer, but again the outcrop line is a streamline and there is no ventilation of the abyssal layer to the south of the outcrop. The geometry of  $z_3$  in the remaining basin is almost flat as in the data. Except in the outcropping region, pressure in the upper layer is proportional to the depth of the  $z_2$  surface, and the resulting upper-layer transport (not shown) has a magnitude of approximately 25 Sv.

Potential vorticity,  $q_2$ , contours are inclined with respect to latitude circles in the eastern basin, as observed in [Fig. 4](#). In the western basin there is a large region of uniform potential vorticity; this induces recirculations against the western boundary of about 1.5 Sv in layer two, as shown in the layer two streamfunction,  $\psi_2$ , in [Fig. 7c](#).

In the unhomogenized case  $z_2$  is virtually indistinguishable from the homogenized case and  $\psi_2$  is zero everywhere; thus we show only  $q_2$  in [Fig. 8](#). These potential vorticity contours are closed against the western boundary, and are more in accordance with [Fig. 4](#), although we now have no subsurface flow in this region.

In reality we suspect that the ocean lies somewhere between the two limiting cases of homogeneous potential vorticity and no flow in the pool region. We therefore choose to explore both limiting cases in the subsequent analysis.

The close match of  $q_2$  (except in the HR in [Fig. 7](#)) to potential vorticity in [Fig. 4](#), and of  $z_2$  to pressure in [Fig. 3](#), supports our hypothesis that it is the wind field that sets the geometry of potential vorticity contours at middepths in the real ocean.

#### e. Sensitivity to model parameters

We have explored the sensitivity of the model fields to  $\gamma_1$  and  $\gamma_2$ . If we increase both  $\gamma_1$  and  $\gamma_2$  by 20%, we find that the maximum depth of the  $z_2$  surface decreases by  $\sim 50$  m, and the HR shrinks  $\sim 1.5^\circ$  in a meridional sense, and  $3^\circ$  zonally. The sensitivity of the model fields may be interpreted as the linear response to small perturbations from the central solution. The qualitative features we have discussed thus far are not altered.

We consider  $\hat{Z}_2 = -600$  m (the depth of the upper layer at the eastern boundary) to be constrained well by hydrography and we do not change this value. In the case of  $\hat{Z}_3$  however we have to choose a value for the lower boundary of the model MW layer. This is somewhat arbitrary since we are unable to recognize a distinct boundary between what we are labeling as the upper and lower MST. The model  $\hat{Z}_3$  depth affects the size of the HR. For  $\hat{Z}_3 = -1400$  m the wind field is less able to distort  $q_2$  contours in layer two and the single closed pool we obtain for  $\hat{Z}_3 = -1300$  m is reduced to a series of small, isolated recirculations against the western boundary. For  $\hat{Z}_3 = -1200$  m the closed pool becomes too large. Since we wish to explore the effect of the homogenization process on the model fields as well as to represent as much of the upper MST as possible, we have chosen  $\hat{Z}_3 = -1300$  m as a best compromise.

An examination of the potential vorticity ( $q_2$ ) field for the upper MST, shown in [Fig. 4](#), reveals  $q_2$  contours sweeping southward and extending westward into the interior from the eastern-boundary slope current. Some of the  $q_2$  contours emanate from the eastern boundary itself. We propose that the MST is able to ventilate the interior ocean along these potential vorticity contours via the narrow eastern boundary current, which travels northward along the coast of Spain and Portugal as a continuation of the MU. We can thus picture water “peeling off” via instability from the eastern boundary current and being carried southwestward along potential vorticity contours, which intersect the eastern boundary as represented schematically in [Fig. 9](#). This physical picture is consistent with the northward spreading of the salinity tongue on  $\sigma_1 = 31.85$ , with salinity on  $\sigma_1 = 32.35$ , where the spreading is more zonal since there is little or no eastern boundary current (and therefore ventilation) at this depth, and also the study of MM99; their results are however based primarily on salinity transports, not mass transports. There is still some uncertainty about the appropriate eastern boundary condition at the depths of the upper MST. [Maze et al. \(1997\)](#), for example, suggest that the mass flux is into the boundary region north of Gibraltar; therefore in practice the detailed distribution of the eastern boundary ventilation may be more complicated.

A flow along potential vorticity contours is obtained by imposing a pressure field at the eastern boundary in a latitude range representative of ventilation by the eastern-boundary current. We choose to impose a piecewise-linear pressure field with outflow from the basin between  $36^\circ\text{N}$  and  $38^\circ\text{N}$  in layer one to represent the surface flow into the Mediterranean Sea, and an inflow of equal and opposite volume transport to the basin between  $36^\circ\text{N}$  and  $51^\circ\text{N}$  in layer two. The latter is supported by observations of MM99. The steady-state solution including homogenization and an inflow at the eastern boundary is found iteratively. Details of the method of solution are given in the appendix.

Convergence occurs for volume transports of  $\sim 0.7$  Sv or less; this is below current estimates for the transport after entrainment by a factor of about 4. The lack of convergence for stronger inflows may suggest that the solution becomes more nonlinear as the eastern boundary ventilation itself distorts the potential vorticity contours significantly. Indeed, this is suggested by the solutions presented in [Spall \(1999\)](#). Here we explore the dynamical controls on the formation of the MST in the weak-inflow limit and scale the mixing coefficient accordingly.

[Figure 10](#) shows  $\psi_2$  and  $q_2$  in the unhomogenized case, for a volume transport of 0.5 Sv. Note that the geometry of the  $q_2$  contours in (a) is barely changed from [Fig. 8](#) by the presence of the inflow. The presence of ventilation in layer two is visible in (b) on the  $\psi_2$  surface. Here  $\psi_2$  and  $q_2$  for the unhomogenized case are not shown. The mean transport generated for this 0.5 Sv case corresponds to a mean velocity of  $\sim 1$  mm s $^{-1}$  in the ventilated region. In the presence of fluctuations over 20 cm s $^{-1}$  in the current meter record of [Zenk and Müller \(1988\)](#) and [Müller and Siedler \(1992\)](#), the difficulty of detecting a mean flow if it is of this order is not surprising. Nevertheless, we shall see shortly how crucially important this weak flow is for the development of the salinity tongue.

### 3. Salinity tongues

The streamfunction field from the wind-driven model is mapped onto a  $1^\circ\text{C}$  grid and used to solve an advection–diffusion equation numerically for the salinity  $S$  in layer two,

$$\nabla \cdot [\overline{hSu} - \overline{hK_S} \nabla S] = 0, (11)$$

using a Gauss–Seidel relaxation method ([Press et al. 1992](#)) since the tracer equation is elliptic at steady state.

Layer two represents a density surface along which salinities representative of MW ( $S = 36.0$  psu), ULSW ( $S = 34.88$  psu), and AAIW ( $S = 34.98$  psu) [values taken from [Lozier et al. \(1995\)](#)] are present. In the derivation of (11) we assume that eddies mix salinity along isopycnals and that this may be parameterized as a Fickian diffusion according to [Gent et al. \(1995\)](#); that is, that  $(\overline{hu})'S' = -\overline{hK_S} \nabla S$ , where  $K_S$  is a downgradient mixing coefficient that represents the action of isopycnal mixing processes that are small in the zero-order potential vorticity balance, but whose effect over long timescales on the salinity field is important. There is some support for this in the numerical experiments of [Lee et al. \(1997\)](#). The work of [Spall \(1994\)](#) does suggest however that the flux of salt in the interior may not be well represented in this form.

AAIW is imposed as a restoring condition on salinity along the southern boundary of the domain, at  $10^\circ\text{N}$ . In our model the southern boundary condition is a strong relaxation to observations as in [Fig. 1a](#), rather than being free to evolve. The large-scale features of the model salinity tongues are not sensitive to the salinity value at the southern boundary, although clearly the complete removal of a restoring condition would have a major impact on the structure of the salinity tongue.

However, in practice water masses have difficulty crossing the equator, and therefore a restoring condition on AAIW seems physically justified.

ULSW and MW are allowed to enter the model domain through boundary currents on the western and eastern sides of the basin, as sketched in [Fig. 11](#). Where eastward flow occurs from the western boundary current the signal of ULSW is able to propagate into the basin; where westward flow occurs MW is absorbed and transported by the boundary current. (We assume that mass closure in layer one is also accomplished by the presence of a western boundary current.) The strengths of the boundary currents are determined through continuity. By balancing the fluxes of salt into and out of the boundary current, and neglecting the storage of water within the boundary current, this allows us to compute the boundary current salinity. (Effectively we are taking the limit in which the boundary layer is infinitely thin.) The western boundary current exists along the entire western boundary of the domain. The eastern boundary current (unless stated otherwise) exists only in the ventilated region between  $38^\circ$  and  $51^\circ\text{N}$ . There is a boundary condition of no normal flow, and no normal gradient in the salinity field along the unventilated region of the eastern boundary and the northern boundary.

The solutions are insensitive to the volume transport of ULSW; there is no detectable difference in the salinity field for a test case in which the volume transport of ULSW along the western boundary is between 5 Sv and 20 Sv.

### *a. Control case with no outflow*

In [Fig. 12](#) we present a control solution using the streamfunction field from [Fig. 7](#) in which we examine the purely diffusive limit of the circulation off the eastern boundary for  $K_S = 100 \text{ m}^2 \text{ s}^{-1}$ . There is no eastern boundary ventilation in this case; however, we prescribe an eastern boundary salinity between  $36^\circ$  and  $51^\circ\text{N}$ . There is no evidence of the tongue-like feature in the salinity field that we see in the data.

### *b. Case with 0.5 Sv outflow*

Salinity fields obtained using the streamfunction from [Fig. 10](#), with a homogenized pool, are shown in [Fig. 13](#) for different values of the mixing coefficient  $K_S$ . The unhomogenized case is shown in [Fig. 14](#). The Peclet number  $P = UL/K_S$ , a measure of the relative importance of advection and mixing, where  $U$  and  $L$  are characteristic velocity and length scales, is given in each case. We choose  $U$  to be the mean velocity of the flow from the boundary current into the interior and  $L$  is the meridional extent of the ventilated boundary current. It is the Peclet number that controls the shape of the salinity tongue, which is a robust feature of the model for different values of  $P$  in both homogenized and unhomogenized cases.

Both the shape of the salinity tongue (particularly for  $P \sim 13$ , where advection dominates over mixing by an order of magnitude) and also its spreading latitude bear much qualitative resemblance to observations as shown in [Fig. 1](#). The homogenization or otherwise of potential vorticity plays a surprisingly small role in determining the shape of the salinity tongues in [Fig. 13](#). The only difference is that in the homogenized case, strongly recirculating ULSW within the closed pool maintains a front against the inward diffusion of MW. In [Fig. 14](#), where there is no homogenized region and accompanying recirculation, there is no front.

For volume transports of varying magnitude, but the same Peclet number, the shape of the salinity tongue is very similar. However, the positions of the salinity contours differ as they are advected farther westward across the basin for greater volume transports. To illustrate this we present a salinity tongue for a volume transport of 0.25 Sv in the homogenized case in [Fig. 15](#) (to be compared with [Fig. 13b](#)). The salinity contours are not advected as far westward as in [Fig. 13b](#), and as a consequence are more realistically positioned with respect to [Fig. 1a](#) in the eastern basin. However, the ventilation in this case is not sufficiently strong to extend the salinity signal to the western reaches of the basin as is observed.

### *c. Mixing coefficient*

The values of mixing coefficient used to produce [Fig. 13](#) ( $K_S = 22, 44, \text{ and } 88 \text{ m}^2 \text{ s}^{-1}$ , respectively) are smaller than current estimates. [Richardson and Mooney \(1975\)](#) estimated lateral mixing coefficients between  $\sim 600 \text{ m}^2 \text{ s}^{-1}$  and  $\sim 5500 \text{ m}^2 \text{ s}^{-1}$ , which would be expected since they used [Stommel's \(1948\)](#) barotropic streamfunction field in which velocities are unrealistically large. [Needler and Heath \(1975\)](#) obtained estimates for  $K_S$  between  $\sim 1500 \text{ m}^2 \text{ s}^{-1}$  and  $\sim 3000 \text{ m}^2 \text{ s}^{-1}$ , and [Armi and Stommel \(1983\)](#) and [Danialt et al. \(1994\)](#) produced estimates of  $\sim 500 \text{ m}^2 \text{ s}^{-1}$ . [Spall et al. \(1993\)](#) obtained zonally enhanced estimates of  $K_{Sx} = 2100 \text{ m}^2 \text{ s}^{-1}$  and  $K_{Sy} = 840 \text{ m}^2 \text{ s}^{-1}$  due to the influence of the  $\beta$  effect in constraining



meridional motions.

Alternatively one can estimate  $K_S$  based on a parameterization derived from baroclinic instability theory ([Green 1970](#); [Stone 1972](#)),

$$K_S = \alpha \frac{\partial z}{\partial x} N l^2, \quad (12)$$

where  $\partial z/\partial x$  is the isopycnal slope,  $N$  is the buoyancy frequency, and  $l$  is a mixing length scale. Here  $\alpha$  is a constant of proportionality, which [Visbeck et al. \(1997\)](#) have determined empirically to be 0.015. We identify the mixing length scale with the Rhines scale,  $(U_1/\beta)^{1/2}$ , where  $U_1$  is a surface velocity.

Taking  $U_1 = 0.1 \text{ m s}^{-1}$  and  $\beta = 2.0 \times 10^{-11} \text{ m}^{-1} \text{ s}^{-1}$ , we obtain  $l = 0.7 \times 10^5 \text{ m}$ . Substituting  $\partial z/\partial x = 1.6 \times 10^{-4}$  (the  $z_2$  surface in [Fig. 7](#) changes by 800 m in  $\sim 5000 \text{ km}$ ),  $N = 2 \times 10^{-3} \text{ s}^{-1}$  [taken from [Chérubin et al. \(1997\)](#)], and  $l = 0.7 \times 10^5 \text{ m}$  into (12), we obtain  $K_S \sim 20 \text{ m}^2 \text{ s}^{-1}$ . This value is too small; however, we note that to obtain a value for  $K_S$  of  $1500 \text{ m}^2 \text{ s}^{-1}$  more in accord with current estimates (by varying  $l$  only), we would require a mixing lengthscale of over 600 km. This may be reasonable *along* potential vorticity contours ([Spall et al. 1993](#)). However, it is predominantly mixing *across* potential vorticity contours that controls the structure of the MST in our model, where velocities are much weaker and the mixing lengthscale will be smaller.

Some of the smallness of  $K_S$  in our model may be attributed to the fact that we are only able to solve for weak inflows. However, even if we could solve for an eastern boundary ventilation of 3 Sv, we would be using  $K_S \sim 200 \text{ m}^2 \text{ s}^{-1}$  to produce a salinity tongue with a Peclet number,  $P \sim 10$ , which is still smaller than current estimates. To emphasize this point, in [Fig. 16](#) we show a salinity tongue computed for a case including 0.5 Sv eastern boundary ventilation and a mixing coefficient,  $K_S = 500 \text{ m}^2 \text{ s}^{-1}$ . The resulting Peclet number is  $P = 1.38$ ; the solution is clearly far too diffusive in comparison to [Fig. 1a](#).

It is known that eddy transports can be advective or diffusive in nature ([Gent et al. 1995](#)); meddies, for instance, can advectively transport fluid across  $q$  contours since they propagate as coherent vortices, often steered by the bottom topography. We conclude that it is unclear how applicable a downgradient diffusive closure is in this region for the transport across potential vorticity contours.

#### d. Solution with no wind forcing

Finally we consider the case of no wind forcing to emphasize the crucial role of the wind field in controlling the geometry of potential vorticity contours and hence the shape of the salinity tongue. In [Fig. 17](#) we show a salinity tongue for the no-wind case and an eastern boundary ventilation of 0.5 Sv. In the absence of the wind field, the potential vorticity contours are zonal and this is reflected in purely zonal flows in layer two. In comparison with [Fig. 14b](#), the salinity tongue spreads too far north and is far less in accord with observations.

## 4. Meddies

We now consider the impact of meddies on the structure of the MST. Meddies adiabatically transfer fluid between the eastern boundary and the interior and therefore provide an eddy thickness, or “bolus,” transport ([Gent et al. 1995](#)),  $\overline{h'u'}$ , where the primes denote departures from the time mean. However, because meddies are coherent vortices that propagate preferentially southwestward, we cannot parameterize the meddy bolus transport in terms of mean layer thickness gradients as in [Gent and McWilliams \(1990\)](#). Instead, we simply prescribe the bolus transports in our model. A similar treatment of meddies has been employed by [Spall \(1998\)](#).

#### a. Meddy-induced recirculation

Meddies are known to be dissipated slowly on the basin scale and also catastrophically by interactions with topography. Where the latter occurs there will be a localized release of water into an isopycnal layer, which we can view as a convergence of the bolus transport. This convergence is analogous to the vertical velocity of the Ekman-pumping field, which drives a southward flow in the subtropical gyre; we expect a modification to the mean flow from the meddy bolus convergence.

Within the zone of meddy convergence a flow is forced across mean potential vorticity contours, and leads to a basin-scale recirculation extending to the western boundary as sketched in [Fig. 18](#) (also see [Pedlosky 1996](#)). A simple scaling predicts the magnitude of the recirculation. We assume that meddies provide a source of water at a rate  $M$  over a region of zonal extent  $L_x$  and meridional extent  $L_y$ . In addition, for simplicity we assume that the potential vorticity gradient is dominated by  $\beta$ . A simple Sverdrup balance yields an equatorward transport,

$$T = \mathbf{v}_g h L_x = \frac{fM}{\beta L_y} = M \frac{R \tan \theta}{L_y}, \quad (13)$$

where  $\mathbf{v}_g$  is the geostrophic velocity and  $h$  is the layer thickness. Note that the strength of the recirculation varies inversely with the meridional extent of the meddy convergence zone,  $L_y$ . Thus localized meddy convergence regions over seamount chains will lead to far greater recirculations than the basin-scale spindown of meddies.

Consider the Great Meteor Seamount chain (which lies directly across the axis of the MST) as a specific example. A meddy 70 km across and 1000 m deep has a volume of  $\sim 3.8 \times 10^{12} \text{ m}^3$ . If we assume that the volume thickness anomaly associated with such a meddy is one-tenth of this, that is,  $3.8 \times 10^{11} \text{ m}^3$ , and that two such meddies are completely dissipated in the region of the GMS chain each year, this is equivalent to a volume flux  $M$  of 0.026 Sv. Taking  $L_x \sim 300$  km,  $L_y \sim 600$  km,  $f \sim 0.7 \times 10^{-4} \text{ s}^{-1}$ , and  $\beta \sim 2 \times 10^{-11} (\text{m s})^{-1}$  yields a transport  $T \sim 0.3 \times 10^6 \text{ m}^3 \text{ s}^{-1}$ . The transport in the recirculation is almost an order of magnitude greater than that of the meddy source. We thus anticipate that strong recirculating mean flows may be generated by even moderate bolus transport convergences due to meddies.

## b. Formulation

### 1) POTENTIAL VORTICITY EQUATION

It remains to represent the effect of the meddy convergence on the mean fields. We do this as follows. The continuity equation in steady state is simply

$$\nabla \cdot [\overline{h'u'} + \overline{hu}] = 0. \quad (14)$$

Substituting geostrophic balance into [\(14\)](#) and rearranging, we obtain

$$\mathbf{k} \times \nabla \left[ \frac{\overline{h}}{\rho_0 f} \right] \cdot \nabla \overline{p}_2 = \nabla \cdot \overline{h'u'}, \quad (15)$$

where  $\mathbf{k} \times \nabla[\overline{h}/f]$  is a characteristic velocity. We compute the change in  $p_2$  by integrating along all  $\overline{h}/f$  contours that pass through a defined area of divergence. The solution is found iteratively in the same way as for the eastern boundary ventilation. Note that we neglect the relative vorticity present in the meddies prior to dissipation.

### 2) SALINITY EQUATION

In the salinity equation we also include an advection by the bolus transport,  $\overline{h'u'}$ ; thus the salinity [\(11\)](#) now becomes

$$\nabla \cdot [\overline{S}(\overline{hu} + \overline{h'u'}) - \overline{h}K_S \nabla \overline{S}] = 0. \quad (16)$$

Thus the salt flux due to the dissipation of meddies (via the convergence of this bolus transport) is explicitly included in our tracer model.

## c. Solutions

We consider a simple example in which we examine the effect of a single region of meddy convergence on the dynamics of the MST. We consider a net convergence of 0.026 Sv, representative of two meddies per year being dissipated by the GMS chain as discussed in the scaling estimate above.

Figure 19 shows the streamfunction in layer two,  $\psi_2$ , and the potential vorticity in layer two,  $q_2$ , in a case with meddies, no homogenized pool, and no eastern boundary ventilation aside from the bolus contribution. The streamfunction is now defined to include the bolus velocity as

$$[\overline{h'u'} + \overline{hu}] = \mathbf{k} \times \nabla \psi_2. (17)$$

The  $\psi_2$  field clearly exhibits a strong anticyclonic recirculation of approximately 0.2 Sv downstream of the patch of divergence shown in (c). The bolus transport,  $\overline{h'u'}$ , is too small to be visible in Fig. 19a and is unable to advect salinity away from the eastern boundary; the resulting salinity tongues (not shown) differ little from Fig. 12. The geometry of the  $q_2$  contours in (b) is again barely changed by the presence of the convergence field. The strength of the recirculation differs slightly from the scaling estimate for a variety of reasons: The size of the region of meddy convergence is larger than in the scaling estimate (for numerical stability), the distribution of the convergence is not uniform, and the potential vorticity gradient is modified from  $\beta$  by layer thickness gradients.

The streamfunction in layer two,  $\psi_2$ , for the same meddy convergence as in Fig. 19, and with the inclusion of an eastern boundary ventilation of 0.5 Sv, is shown in Fig. 20. There are now many streamlines emanating from the eastern boundary into the interior. The resulting steady salinity distribution for this streamfunction field is shown in Fig. 21 for a mixing coefficient,  $K_S = 50 \text{ m}^2 \text{ s}^{-1}$ . The ventilation process transports salinity to the recirculation in the interior much more efficiently than the bolus transport; the recirculation is then able to advect salinity contours around, modifying the salinity tongue from Fig. 14b (the equivalent figure in the absence of meddies) by shifting the axis of the tongue southward.

This study is somewhat abstract in that we consider only a single patch of dissipation, whereas in reality there are likely to be many such patches of enhanced dissipation, separated by larger regions of weak decay. Nevertheless, it illustrates an important concept, which is that of the strong anticyclonic recirculation. It appears that the net effect of many such recirculations would be to shift the tongue southward.

## 5. Discussion

We have presented a simple 2.5-layer planetary geostrophic model of the North Atlantic to study the impact of the surface winds, eastern boundary ventilation, and meddies on the structure of the Mediterranean salinity tongue (MST). The geometry of the upper-layer depth is controlled by the wind field and exhibits a clear similarity to climatology. This defines the potential vorticity in the second layer, at the depth of the upper MST, and sets up the free pathways for the spreading of MW. The shape and spreading latitude of the model salinity tongues bear a striking resemblance to the observed upper MST. The salinity tongues are remarkably stable to variations in the Peclet number.

We observe a frontal zone between the MW and ULSW in the salinity fields of the limit in which we homogenize potential vorticity within closed contours, leading to a recirculation of ULSW into the interior. There is a frontal zone in the salinity field on the  $\sigma_1 = 32.35$  surface (Fig. 1) around  $40^\circ$ – $50^\circ\text{N}$  between the MW and ULSW that appears to be due to the eastward propagation of ULSW around  $50^\circ\text{N}$  (as inferred by Talley and McCartney 1982), but not on the  $\sigma_1 = 31.85$  surface. This would suggest that the flow at the depths of the upper MST in this region is weak and more akin to the unhomogenized scenario. Nevertheless, there is remarkably little difference in the geometry of the salinity tongues between cases with and without homogenization.

The presence of a mean transport away from the eastern boundary by ventilation from the boundary current is a crucial factor in our model in transporting salinity away from the eastern boundary. These transports correspond to mean velocities in the model of  $\sim 1 \text{ mm s}^{-1}$ , but if they are not included one obtains a grossly unrealistic salinity tongue, as shown in Fig. 12. Our model produces no northward interior flow in the ventilated region, at odds with the estimate of Saunders (1982). However the more recent inverse calculation of Paillet and Mercier (1997) shows little mean flow at the depths of the upper MST.

We have included a simple parameterization of meddies as distributed mass sources in the second layer, for example, arising from collisions of meddies with seamounts. These can drive large mean recirculations extending across to the western boundary; their net effect is to shift the salinity tongue southward.

We have not considered the dynamics of the lower MST, at the depths of which there is little or no ventilation from the eastern boundary or meddies. Double diffusive processes appear to be important here in extending the salinity signal downward from the base of the upper MST. This idea has been investigated recently by Spall (1999), who suggests that the southward recirculation of ULSW at the depths of the lower MST is, at least in part, driven by double-diffusive mixing, in a

manner similar to the recirculation driven by meddies in our model. There is an additional dynamic feedback on the upper MST, which implies a northward flow by vortex stretching, although its importance is still unclear.

Nevertheless, the success of our model in producing realistic salinity tongues suggests that the zero-order dynamical balance within the upper MST may be adiabatic, as implied by the work of [Richardson and Mooney \(1975\)](#). As such we would expect such additional diapycnal effects to represent a modification to the picture we have presented.

### Acknowledgments

The authors wish to thank Mike Spall, Jerome Paillet, Eric Kunze, Peter Killworth, and an anonymous reviewer for numerous useful comments at the reviewing stage. Thought provoking discussions with Steve Meacham, Mike Spall, and Mike McCartney prior to submission are also acknowledged. Many thanks are also expressed to Ruth Curry for supplying [Figs. 1](#), [3](#), and [4](#), and Jerome Paillet for supplying [Fig. 2](#). A Reading University Endowment Fellowship and NERC Grant GR8/03760 are acknowledged.

---

### REFERENCES

- Arhan, M., 1987: On the large scale dynamics of the Mediterranean Outflow. *Deep-Sea Res.*, **34**, 1187–1208..
- , A. Colin de Verdière, and L. Mémery, 1994: The eastern boundary of the subtropical North Atlantic. *J. Phys. Oceanogr.*, **24**, 1295–1316.. [Find this article online](#)
- Armi, L., and D. Haidvogel, 1982: Effects of variable and anisotropic diffusivities in a steady state diffusion model. *J. Phys. Oceanogr.*, **12**, 785–794.. [Find this article online](#)
- , and H. Stommel, 1983: Four views of a portion of the North Atlantic subtropical gyre. *J. Phys. Oceanogr.*, **13**, 828–857.. [Find this article online](#)
- , D. Herbert, N. Oakey, and J. Price, 1989: Two years in the life of a Mediterranean salt lens. *J. Phys. Oceanogr.*, **19**, 354–370.. [Find this article online](#)
- Baringer, M. O., and J. F. Price, 1997a: Mixing and spreading of the Mediterranean outflow. *J. Phys. Oceanogr.*, **27**, 1654–1677.. [Find this article online](#)
- , and —, 1997b: Momentum and energy balance of the Mediterranean outflow. *J. Phys. Oceanogr.*, **27**, 1678–1692.. [Find this article online](#)
- Bower, A. S., L. Armi, and I. Ambar, 1995: Direct evidence of meddy formation off the southwestern coast of Portugal. *Deep-Sea Res.*, **42**, 1621–1630..
- , —, and —, 1997: Lagrangian observations of Meddy formation during a Mediterranean Undercurrent seeding experiment. *J. Phys. Oceanogr.*, **27**, 2545–2575.. [Find this article online](#)
- Chérubin, L., A. Serpette, X. Carton, and J. Paillet, 1997: Descriptive analysis of the hydrology and currents on the Iberian shelf from Gibraltar to Cape Finisterre: Preliminary results from the SEMANE and INTERAFOS experiments. *Ann. Hydrograph.*, **21** (768), 5–69..
- Curry, R. G., 1996: Hydrobase: A database of hydrographic stations and tools for climatologic analysis. Woods Hole Oceanographic Institution Tech Rep. 96-01, 50 pp. [Available from Woods Hole Oceanographic Institution, Woods Hole, MA 02543.].
- Daniault, N., J. P. Maze, and M. Arhan, 1994: Circulation and mixing of Mediterranean Water west of the Iberian Peninsula. *Deep-Sea Res.*, **41**, 1685–1714..
- D’Asaro, E. A., 1988: Generation of submesoscale vortices: A new mechanism. *J. Geophys. Res.*, **93**, 6685–6693..
- DaSilva, A., A. C. Young, and S. Levitus, 1994: NOAA SMD94. Tech. Rep. 6, NOAA/NESDIS, Washington, DC, 83 pp..
- Gent, P. R., and J. C. McWilliams, 1990: Isopycnal mixing in ocean circulation models. *J. Phys. Oceanogr.*, **20**, 150–155.. [Find this article online](#)
- , J. Willebrand, T. J. McDougall, and J. C. McWilliams, 1995: Parameterizing eddy-induced transports in ocean circulation models. *J. Phys. Oceanogr.*, **25**, 463–474.. [Find this article online](#)
- Green, J. S., 1970: Transfer properties of the large-scale eddies and the general circulation of the atmosphere. *Quart. J. Roy. Meteor. Soc.*,

- Howe, M. R., 1984: Current and hydrographical measurements in the Mediterranean Undercurrent near Cape St. Vincent. *Oceanol. Acta*, **7**, 163–168..
- Kase, R. H., and W. Zenk, 1996: The structure of the Mediterranean water and meddy characteristics in the northeastern Atlantic. *The Warmwatersphere of the North Atlantic*, Gebrüder Borntraeger..
- Lacombe, H., 1971: Le détroit de Gibraltar océanographie physique. Extrait de: Mémoire explicatif de la Carte géotechnique de Tanger au 1/25 000. *Notes M. Serv. Geol. Maroc*, **222**, 111–146..
- Lee, M., D. P. Marshall, and R. G. Williams, 1997: On the eddy transfer of tracers: Advective or diffusive? *J. Mar. Res.*, **55**, 483–505..
- Lozier, M. S., W. B. Owens, and R. G. Curry, 1995: The climatology of the North Atlantic. *Progress in Oceanography*, Vol. 36, Academic Press, 1–44..
- Luyten, J. R., J. Pedlosky, and H. Stommel, 1983: The ventilated thermocline. *J. Phys. Oceanogr.*, **13**, 292–309.. [Find this article online](#)
- Maze, J. P., M. Arhan, and H. Mercier, 1997: Volume budget of the eastern boundary layer off the Iberian Peninsula. *Deep-Sea Res.*, **44**, 1543–1574..
- McDowell, S. E., and H. T. Rossby, 1978: Mediterranean Water: An intense mesoscale eddy off the Bahamas. *Science*, **202**, 1085–1087..
- Müller, T. J., and G. Siedler, 1992: Multiyear current time-series in the eastern North Atlantic Ocean. *J. Mar. Res.*, **50**, 63–98..
- Needler, G. T., and R. A. Heath, 1975: Diffusion coefficients calculated from the Mediterranean salinity anomaly in the North Atlantic Ocean. *J. Phys. Oceanogr.*, **5**, 173–182.. [Find this article online](#)
- Paillet, J., and H. Mercier, 1997: An inverse model of the eastern North Atlantic general circulation and thermocline ventilation. *Deep-Sea Res.*, **44**, 1293–1328..
- Pedlosky, J., 1996: *Ocean Circulation Theory*. Springer-Verlag, 453 pp..
- Press, W. H., S. A. Teukolsky, W. T. Vetterling, and B. P. Flannery, 1992: *Numerical Recipes in FORTRAN. The Art of Scientific Computing*. Cambridge University Press, 989 pp..
- Reid, J. L., 1979: On the contribution of the Mediterranean Sea outflow to the Norwegian–Greenland Sea. *Deep-Sea Res.*, **26A**, 1199–1223..
- Rhines, P. B., and W. R. Young, 1982a: Homogenization of potential vorticity in planetary gyres. *J. Fluid Mech.*, **122**, 347–368..
- , and —, 1982b: A theory of the wind-driven circulation. Part 1: Mid-ocean gyres. *J. Mar. Res.*, **40**, 559–596..
- Richardson, P. L., and K. Mooney, 1975: The Mediterranean Outflow—A simple advection–diffusion model. *J. Phys. Oceanogr.*, **5**, 476–482.. [Find this article online](#)
- , and A. Tychensky, 1998: Semaphore meddy trajectories. *J. Geophys. Res.*, **103**, 25 029–25 045..
- , D. Walsh, and L. Armi, 1989: Tracking three meddies with SOFAR floats. *J. Phys. Oceanogr.*, **19**, 371–383.. [Find this article online](#)
- , M. S. McCartney, and C. Maillard, 1991: A search for meddies in historical data. *Dyn. Atmos. Oceans*, **15**, 241–265..
- Saunders, P. M., 1982: Circulation in the eastern North Atlantic. *J. Mar. Res.*, **40** (Suppl), 641–651..
- Schopp, R., and M. Arhan, 1986: A ventilated mid-depth circulation model for the eastern North Atlantic. *J. Phys. Oceanogr.*, **16**, 344–357.. [Find this article online](#)
- Shapiro, G. I., S. L. Meschanov, and M. V. Emelianov, 1995: Mediterranean lens “Irving” after its collision with seamounts. *Oceanol. Acta.*, **18**, 309–318..
- Spall, M. A., 1994: Mechanism for low-frequency variability and salt-flux in the Mediterranean salt tongue. *J. Geophys. Res.*, **99**, 10 121–10 129..
- , 1999: A simple model of the large scale circulation of Mediterranean Water and Labrador Sea Water. *Deep Sea Res.*, **46**, 181–204..
- , P. L. Richardson, and J. Price, 1993: Advection and eddy mixing in the Mediterranean salt tongue. *J. Mar. Res.*, **51**, 797–818..



Stommel, H., 1948: The westward intensification of wind-driven ocean currents. *Trans. Amer. Geophys. Union*, **29**, 202–206..

Stone, P., 1972: A simplified radiative–dynamical model for the static stability of rotating atmospheres. *J. Atmos. Sci.*, **29**, 405–418.. [Find this article online](#)

Talley, L. D., and M. S. McCartney, 1982: Distribution and circulation of Labrador Sea Water. *J. Phys. Oceanogr.*, **12**, 1189–1205.. [Find this article online](#)

Tziperman, E., 1987: The Mediterranean Outflow as an example of deep buoyancy-driven flow. *J. Geophys. Res.*, **92** (C13), 14 510–14 520..

Visbeck, M., J. Marshall, T. Haine, and M. Spall, 1997: Specification of eddy transfer coefficients in coarse-resolution ocean circulation models. *J. Phys. Oceanogr.*, **27**, 381–402.. [Find this article online](#)

Zenk, W., and T. J. Müller, 1988: Seven-year current meter record in the eastern North Atlantic. *Deep-Sea Res.*, **35**, 1259–1268..

—, and L. Armi, 1990: The complex spreading of Mediterranean Water off the Portuguese continental slope. *Deep-Sea Res.*, **37**, 1805–1823..

---

## APPENDIX A

### 6. Method of Solution

In the cases with eastern-boundary ventilation and/or meddies, the steady-state solutions for the dynamical fields are determined numerically through the following iterative procedure on a  $1/12^\circ$  grid; this high resolution ensures the solutions converge numerically.

1. Initially we assume no flow in layer two.
2. [Equation \(7\)](#) is integrated across the basin from the eastern boundary to determine the geometry of  $z_2$ .
3. Values of  $\hat{Z}_3$  and  $\hat{Z}_2$  for the desired eastern-boundary ventilation are determined from [\(B7\)](#), [\(B8\)](#), and [\(B9\)](#) in appendix B.
4. In the case where there are no meddies, the values of  $\hat{Z}_3$  are then imposed along layer two potential vorticity contours; in the case where we include meddies, this is achieved by integrating along layer two potential vorticity contours (from the previous iteration) by the method of characteristics.
5. Potential vorticity in layer two is updated.
6. Steps 2–5 are repeated until convergence is obtained.
7. Homogenization of potential vorticity is conducted if required according to (10).

For the tracer model, these fields are mapped onto a  $1^\circ$  grid.

---

## APPENDIX B

### 7. Eastern Boundary Ventilation

The volume transport through the eastern boundary,  $V_n$ , where  $n$  is a layer index, is given by (neglecting changes in  $f$ )

In layers one and two this yields

$$\begin{aligned} V_1 &= -\frac{\gamma_1}{2f} [\hat{Z}_2^2]_{\theta(S)}^{\theta(N)} - \frac{\gamma_2}{f} \int_{\theta(S)}^{\theta(N)} \hat{Z}_2 \frac{\partial \hat{Z}_3}{\partial \theta} d\theta, \\ V_2 &= -\frac{\gamma_2}{2f} [\hat{Z}_3^2]_{\theta(S)}^{\theta(N)} + \frac{\gamma_2}{f} \int_{\theta(S)}^{\theta(N)} \hat{Z}_2 \frac{\partial \hat{Z}_3}{\partial \theta} d\theta. \end{aligned} \quad (\text{B2})$$

We assume that both  $\hat{Z}_2$  and  $\hat{Z}_3$  are linear in  $\theta$ ; that is,

$$\frac{\partial \hat{Z}_j}{\partial \theta} = \frac{[\hat{Z}_j(\theta) - \hat{Z}_j(\theta(S))]}{\theta - \theta(S)}, \quad (\text{B3})$$

where  $j$  refers to the surface (2 or 3). Thus,

$$\frac{\gamma_2}{f} \int_{\theta(S)}^{\theta(N)} \hat{Z}_2 \frac{\partial \hat{Z}_3}{\partial \theta} d\theta = \frac{\gamma_2}{f} \frac{[\hat{Z}_3(\theta) - \hat{Z}_3(\theta(S))]}{\theta - \theta(S)} \int_{\theta(S)}^{\theta(N)} \hat{Z}_2 d\theta. \quad (\text{B4})$$

Now,

$$\int_{\theta(S)}^{\theta(N)} \hat{Z}_2 d\theta = \frac{\theta - \theta(S)}{2} [\hat{Z}_2(\theta(N)) + \hat{Z}_2(\theta(S))]. \quad (\text{B5})$$

Hence, combining (B4) and (B5),

$$\begin{aligned} &\frac{\gamma_2}{f} \int_{\theta(S)}^{\theta(N)} \hat{Z}_2 \frac{\partial \hat{Z}_3}{\partial \theta} d\theta \\ &= [\hat{Z}_3(\theta(N)) - \hat{Z}_3(\theta(S))] [\hat{Z}_2(\theta(N)) + \hat{Z}_2(\theta(S))]. \end{aligned} \quad (\text{B6})$$

Finally, substituting (B6) into (B2) we obtain the volume transports

$$\begin{aligned} V_1 &= -\frac{\gamma_1}{2f} [\hat{Z}_2^2]_{\theta(S)}^{\theta(N)} \\ &\quad - \frac{\gamma_2}{2f} [\hat{Z}_3(\theta(N)) - \hat{Z}_3(\theta(S))] [\hat{Z}_2(\theta(N)) + \hat{Z}_2(\theta(S))], \\ V_2 &= -\frac{\gamma_2}{2f} [\hat{Z}_3^2]_{\theta(S)}^{\theta(N)} \\ &\quad + \frac{\gamma_2}{2f} [\hat{Z}_3(\theta(N)) - \hat{Z}_3(\theta(S))] [\hat{Z}_2(\theta(N)) + \hat{Z}_2(\theta(S))]. \end{aligned} \quad (\text{B7})$$

Since we require the layer one flow between 36°N and 38°N and the layer two flow between 36°N and 51°N, we have

two regions of flow through the eastern boundary in which to apply (B7). In region one between 36°N and 38°N we choose the required volume transport in layer one and apportion the layer two flow as

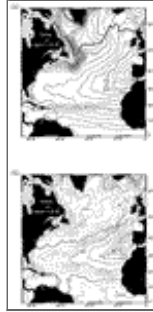
$$V_2(1) = -\frac{38 - 36}{51 - 36}V_1(1), \quad (\text{B8})$$

where  $V_2(1)$  refers to the layer 2 flow in region 1 and  $V_1(1)$  refers to the layer 1 flow in region 1. Since  $\hat{Z}_2(\theta(S))$  and  $\hat{Z}_3(\theta(S))$  are just the resting layer depths, we can solve (B7) for the two unknowns,  $\hat{Z}_3(\theta(N))$  and  $\hat{Z}_2(\theta(N))$ . In region two between 38°N and 51°N we have  $V_1(2) = 0$ ,

$$V_2(2) = -\frac{51 - 38}{51 - 36}V_1(1), \quad (\text{B9})$$

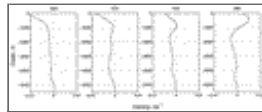
and  $\hat{Z}_2(\theta(S))$  and  $\hat{Z}_3(\theta(S))$  are just  $\hat{Z}_3(\theta(N))$  and  $\hat{Z}_2(\theta(N))$  from region one. We determine  $\hat{Z}_2$  and  $\hat{Z}_3$  between  $\theta(N)$  and  $\theta(S)$  by linear interpolation. This is almost equivalent (since we have taken  $f$  to be constant) to a constant volume transport between adjacent layer two potential vorticity contours at the eastern boundary.

## Figures



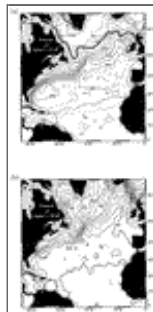
[Click on thumbnail for full-sized image.](#)

Fig. 1. Salinity (psu) on (a)  $\sigma_1 = 31.85$  and (b)  $\sigma_1 = 32.35$ . Reproduced from [Lozier et al. \(1995\)](#).



[Click on thumbnail for full-sized image.](#)

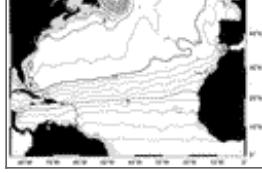
Fig. 2. Section-averaged current profiles computed from the data of Paillet and Mercier (1997) for latitudes 32°–48°N. Positive velocities imply northward flow. Provided by J. Paillet.



[Click on thumbnail for full-sized image.](#)

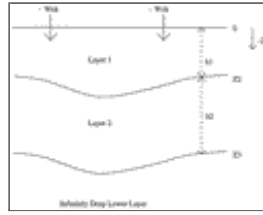
Fig. 3. Pressure (db) on (a)  $\sigma_1 = 31.85$ , (b)  $\sigma_1 = 32.35$ . Reproduced from [Lozier et al. \(1995\)](#).





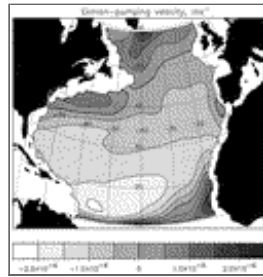
[Click on thumbnail for full-sized image.](#)

Fig. 4. Potential vorticity contours on the  $\sigma_1 = 31.8$  surface. Provided by R. Curry ([Curry 1996](#)).



[Click on thumbnail for full-sized image.](#)

Fig. 5. Schematic of model configuration consisting of two moving layers of thickness  $h_1$  and  $h_2$  overlying a motionless abyss and forced by an Ekman pumping field,  $w_{\text{Ek}}$ . The depths of the interfaces are  $z_2$  and  $z_3$ , respectively.



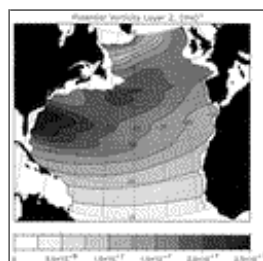
[Click on thumbnail for full-sized image.](#)

Fig. 6. Ekman pumping field ( $\text{m s}^{-1}$ ) derived from seasonally averaged Da Silva (1994) climatology (smoothed with a 9-point moving average filter of order 10 to remove small-scale features not consistent with the model dynamics).



[Click on thumbnail for full-sized image.](#)

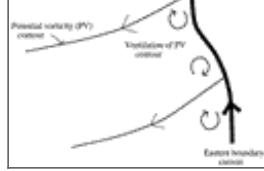
Fig. 7. (a)  $z_2$ , (b)  $q_2$ , and (c)  $\psi_2$  for  $\gamma_1 = 0.005 \text{ m s}^{-2}$ ,  $\gamma_2 = 0.0025 \text{ m s}^{-2}$ ,  $\hat{Z}_2 = -600 \text{ m}$ , and  $\hat{Z}_3 = -1300 \text{ m}$  (homogenized case).



[Click on thumbnail for full-sized image.](#)

Fig. 8. Here  $q_2$  for  $\gamma_1 = 0.005 \text{ m s}^{-2}$ ,  $\gamma_2 = 0.0025 \text{ m s}^{-2}$ ,  $\hat{Z}_2 = -600 \text{ m}$ , and  $\hat{Z}_3 = -1300 \text{ m}$  (unhomogenized case).





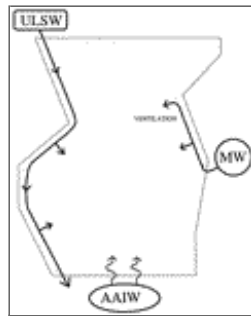
Click on thumbnail for full-sized image.

Fig. 9. Schematic representing hypothesized ventilation process from the eastern boundary current, which occurs onto interior potential vorticity contours acting as free pathways for the flow.



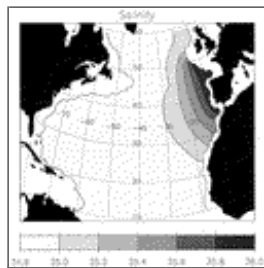
Click on thumbnail for full-sized image.

Fig. 10. (a)  $\psi_2$  and (b)  $q_2$  for  $\gamma_1 = 0.005 \text{ m s}^{-2}$ ,  $\gamma_2 = 0.0025 \text{ m s}^{-2}$ ,  $\hat{Z}_2 = -600 \text{ m}$ , and  $\hat{Z}_3 = -1300 \text{ m}$  for eastern boundary ventilation of 0.5 Sv (homogenized case).



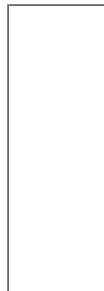
Click on thumbnail for full-sized image.

Fig. 11. A schematic diagram indicating the water mass sources in our tracer model. Mediterranean Water (MW) and Upper Labrador Sea Water (ULSW) enter the model domain through boundary currents on eastern and western sides of the model domain. Antarctic Intermediate Water (AAIW) enters diffusively through the southern boundary.



Click on thumbnail for full-sized image.

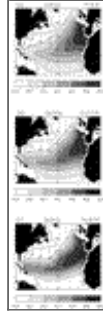
Fig. 12. Salinity field (ppt) obtained with no motion in layer two (homogenized case);  $K_S = 100 \text{ m}^2 \text{ s}^{-1}$ .





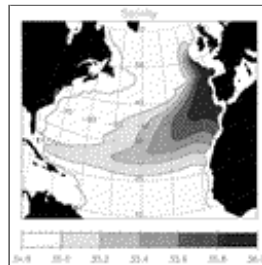
[Click on thumbnail for full-sized image.](#)

Fig. 13. Salinity fields (psu) for 0.5 Sv eastern boundary ventilation (homogenized case) for different Peclet numbers: (a)  $P = 13.8$ , (b)  $P = 27.8$ , (c)  $P = 6.9$ .



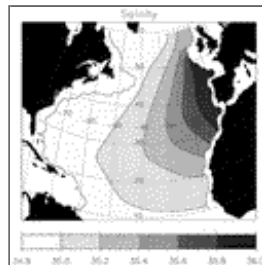
[Click on thumbnail for full-sized image.](#)

Fig. 14. Salinity fields (ppt) for 0.5 Sv eastern boundary ventilation (unhomogenized case): (a)  $P = 13.8$  (b)  $P = 27.8$ , (c)  $P = 6.9$ .



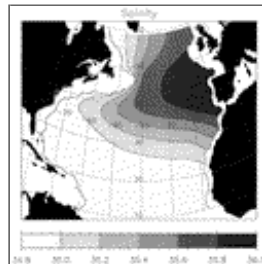
[Click on thumbnail for full-sized image.](#)

Fig. 15. Salinity field (psu) for 0.25 Sv eastern boundary ventilation (homogenized case):  $P = 13.8$ .



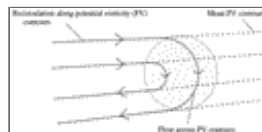
[Click on thumbnail for full-sized image.](#)

Fig. 16. Salinity field (psu) for 0.5 Sv eastern boundary ventilation (homogenized case):  $P = 1.38$ .



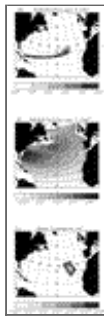
[Click on thumbnail for full-sized image.](#)

Fig. 17. Salinity field (psu) for 0.5 Sv eastern boundary ventilation with no surface winds:  $P = 13.8$ .



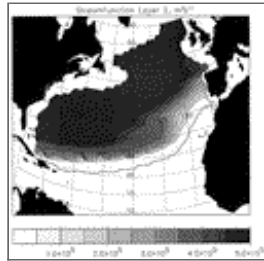
[Click on thumbnail for full-sized image.](#)

Fig. 18. Schematic illustrating basin-scale recirculation directed equatorward across mean potential vorticity contours, generated by meddy convergence (shaded region).




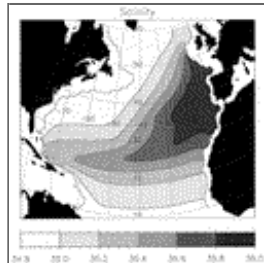
[Click on thumbnail for full-sized image.](#)

Fig. 19. Experiment with 0.026 Sv integrated convergence of meddy bolus transport over Great Meteor Seamount chain: (a)  $\psi_2$ , (b)  $q_2$ , and (c) convergence of meddy bolus transport for  $\gamma_1 = 0.005 \text{ m s}^{-2}$ ,  $\gamma_2 = 0.0025 \text{ m s}^{-2}$ ,  $\hat{Z}_2 = -600 \text{ m}$ , and  $\hat{Z}_3 = -1300 \text{ m}$  (unhomogenized case).




[Click on thumbnail for full-sized image.](#)

Fig. 20. Streamfunction in layer two,  $\psi_2$ , for meddy convergence as in [Fig. 19](#) , and eastern boundary ventilation of 0.5 Sv (unhomogenized case).



[Click on thumbnail for full-sized image.](#)

Fig. 21. Steady salinity field (psu) for meddy convergence as in [Fig. 19](#) , and eastern boundary ventilation of 0.5 Sv (unhomogenized case).

*Corresponding author address:* James C. Stephens, Department of Meteorology, University of Reading, P.O. Box 243, Reading RG6 6BB, United Kingdom.

E-mail: [swrsteph@met.reading.ac.uk](mailto:swrsteph@met.reading.ac.uk)

[top](#) 



